3-Substituted-2,3-Dihydrothiazole as a promising scaffold to design EGFR inhibitors

Radwan El-Haggar, Sherif Hammad, Reem Alsantali, Munira Alrooqi, Mahmoud El Hassab, Nicolas Masurier, Marwa Ahmed

3-Substituted-2,3-Dihydrothiazole as a Promising Scaffold to design EGFR Inhibitors

Radwan El-Haggar[1,2*], Sherif F. Hammad[1,3], Reem I. Alsantali[4], Munira M. Alrooqi[5], Mahmoud A. El Hassab[6], Nicolas Masurier[2*], Marwa F. Ahmed[1,4*]

[1]*Department of Pharmaceutical Chemistry, Faculty of Pharmacy, Helwan University, Ain Helwan 11795, Cairo, Egypt.*

[2]*Institut des Biomolécules Max Mousseron (IBMM), UMR 5247, CNRS, Université de Montpellier, ENSCM, 34293 Montpellier, France.*

[3]*Basic and Applied Science Institute, Egypt-Japan University of Science and Technology (E-JUST), New Borg El-Arab City 21934, Alexandria, Egypt.*

[4]*Department of Pharmaceutical Chemistry, College of Pharmacy, Taif University, P.O. Box 11099, Taif 21944, Saudi Arabia.*

[5]*Department of Chemistry, Faculty of Applies Science, Umm Al-Qura University, 21944, Makkah, Saudi Arabia.*

[6]*Department of Medicinal Chemistry, Faculty of Pharmacy, King Salman International University (KSIU), South Sinai, Egypt.*

Keywords: Hydrazinothiazole, kinase inhibitors, EGFR, colorectal cancer

* **Corresponding authors**:

e-mail addresses: radwan_elhaggar@pharm.helwan.edu.eg (Radwan El-Haggar), nicolas.masurier@umontpellier.fr (Nicolas Masurier), marwafarag80@yahoo.com (Marwa F. Ahmed)

Abstract

The overexpression of EGFR has been recognized as the driver mechanism in the development of several human malignancies and the clinical use of EGFR inhibitors currently constitutes the standard of care for a wide range of malignancies, including colorectal cancer. However, the clinical efficacy of EGFR targeted

inhibitors is limited by the development of intrinsic or acquired resistance, requiring the discovery of new compounds with different structural characteristics from those already developed. In this context, we explored the replacement of the aminoquinazoline pharmacophore of several FDA-approved EGFR inhibitors by its bioisosteric hydrazinothiazole moiety. A series of 14 new compounds were designed, synthesized, and evaluated as potential EGFR inhibitors. Compound **5i** was active against 12 different cell lines in the NCI-60 cell line panel and showed an IC_{50} of 6.9 ± 0.013 µM against HCT-116 cells, with no significant toxicity against normal human fibroblasts (WI-38). Further studies showed that this compound showed submicromolar activity against EGFR and was able to induce tumor cell cycle arrest and cell apoptosis. Additionally, docking experiments, molecular dynamics and binding free energy calculations were performed and confirmed the potential of 2-hydrazino-2,3-dihydrothiazole derivatives as new EGFR inhibitors.

1. Introduction

Colorectal cancer (CRC) has a high incidence and is the fourth leading cause of death worldwide [1]. There are several methods for colon cancer treatments that include polypectomy and surgery, radiation therapy, conventional chemotherapy, and targeted therapy; its therapeutic management depending on its stage of development [2]. However, stage IV, corresponding to metastatic colorectal cancer (mCRC), remains currently incurable.

The understanding of biological mechanisms at the basis of the disease and the discovery of molecular pathways leading to CRC progression have shown that 60 to 80% of mCRC were accompanied with EGFR (Epidermal Growth Factor Receptor) alteration [3]. EGFR is a trans-membrane glycoprotein with a cytoplasmic tyrosine kinase domain and an extracellular ligand-binding domain. Also, EGFR is a member of a family of four main receptor tyrosine kinases that plays a key role in cell signaling pathways that include cell proliferation and apoptosis [4]. These data support the idea that EGFR expression is disrupted in several human malignancies, including CRC. The discovery of EGFR overexpression in cancer has resulted in significant attempts to target the EGFR as a cancer therapy approach during the last four decades [5–8]. Numerous EGFR inhibitors have been reported to date, such as

the Food and Drug Administration (FDA) approved Lapatinib, Gefitinib and Erlotinib [9]. These compounds were widely used in the clinic and are effective in different types of malignancies, including lung, breast, prostate and CRC [10]. Unfortunately, long exposure to these molecules leads to the development of resistance [11]. Thus, to solve this problem, the discovery or development of new structural types of kinase inhibitors is of critical importance.

Different scaffolds have been developed to act as hinge binders in the ATP-binding site of kinases [12]. Fused six-membered ring systems, such as quinazoline and (iso)quinoline, present notably in the structure of Gefitinib, Lapatinib and Erlotinib, were commonly the most used ATP mimetics. Among other studied heterocyclic systems, aminopyrimidine and closely related aminopyridine, pyrrolopyrimidine and pyrrolopyridine moiety have also remained frequently used hinge binders. The amino-thiazole moiety has also been reported to access kinase inhibitors, leading to the discovery of therapeutically approved antitumor drugs like dabrafenib [13] and dasatinib [14]. While present in many compounds with biological activity and readily accessible, its structurally close 2-hydrazinothiazole analog has only been little studied to design kinase inhibitors [15]. Indeed, some biological activities of hydrazinothiazole compounds were identified throughout the years, including anti-arthritic activity [16], antioxidant [17], antifungal [18], antiparasitic activity [19,20], antitubercular [21,22], anticancer activity [23,24], etc.

Thus, to increase the chemical diversity of kinase inhibitors, we report herein the design and synthesis of a series of potential EGFR inhibitors based on the 2-hydrazinothiazole moiety. All of the targeted compounds were tested in vitro for anticancer efficacy against a broad panel of cancer cell lines, including the HCT-116 colon cancer cell line. The EGFR enzymatic inhibitory capability of the synthesized compounds was assessed for further exploration of the putative anticancer mechanism, followed by DNA cell cycle analysis for the most potent derivatives. Also, their cytotoxicity in normal human fibroblasts (WI-38) and capacity to trigger apoptosis were investigated. The levels of mitochondrial anti-apoptotic protein Bcl-2 and pro-apoptotic protein Bax were measured in the HCT-116 cancer cell line. Finally, using Erlotinib as a reference ligand, the synthesized compounds were subjected to molecular docking and dynamic investigations against EGFR.

2. Results and discussion

2.1. Strategy for the compounds design

Our research focuses on the design of novel compounds with comparable essential pharmacophoric properties of EGFR inhibitors, incorporating a 2-hydrazino-2,3-dihydrothiazole moiety as the main core of the inhibitor. The following are the common pharmacophoric features of EGFR inhibitors [25–27]: 1) a flat heteroaromatic system occupying the hydrophobic adenine binding pocket and forming hydrogen bonds to the kinase hinge segment, 2) a hydrophobic terminal head and 3) a hydrophobic tail (Figure 1). Here, the aminoquinazoline moiety (heteroaromatic system) of Erlotinib was substituted by a 2-hydrazinothiazole moiety as a biological isostere. The terminal ethynylphenyl ring (hydrophobic head) was replaced by various substituted phenyl derivatives and finally, the two 2-methoxyethoxygroups (hydrophobic tail) was substituted by a methoxyphenyl ring (Figure 1).

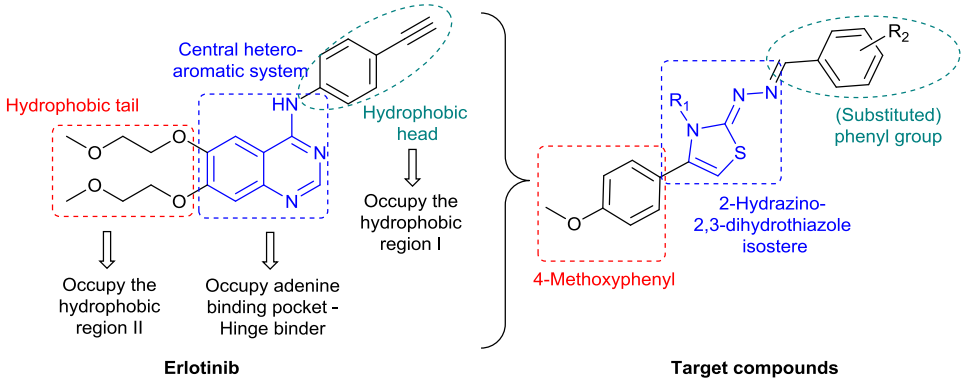

Fig. 1: Erlotinib's core structural characteristics and design of new EGFR inhibitors.

The designed compounds were superimposed with the control drug Erlotinib in the ATP-binding pocket of EGFR (PDB: 1M17). They were seen to bind in a similar conformation as the positive drug, as shown in Figure 2. This demonstrated that the designed compounds with a 2-hydrazino-2,3-dihydrothiazole structure could be used to construct novel EGFR kinase inhibitors.

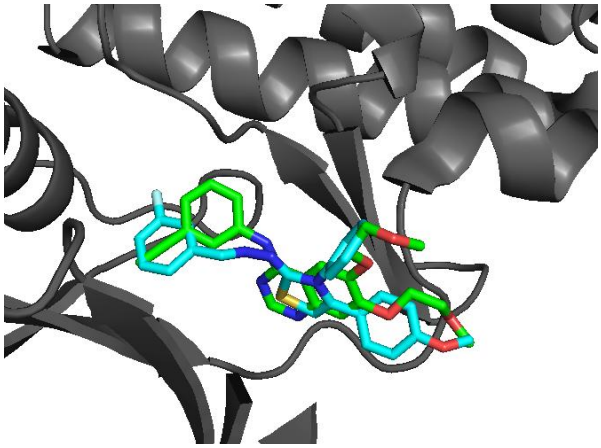

Fig. 2: Superimposed structures of target compounds (cyan) with Erlotinib (green) in the binding pocket of EGFR (PDB: 1M17).

2.2. Chemistry

The synthesis of the target compounds **5a-n** was started by reaction of isothiocyanates **1a-b** with hydrazine hydrate to produce the corresponding thiosemicarbazide **2a-b**. The intermediate thiosemicarbazones **3a-n** were synthesized by reacting the appropriate aldehyde with the thiosemicarbazide **2a-b** in the presence of a catalytic amount of HCl. These intermediates were subsequently reacted with 2-bromo-1-(4-methoxyphenyl)ethan-1-one **4** to produce the **5a-n** series with yields ranging from 60% to 85% (Scheme 1).

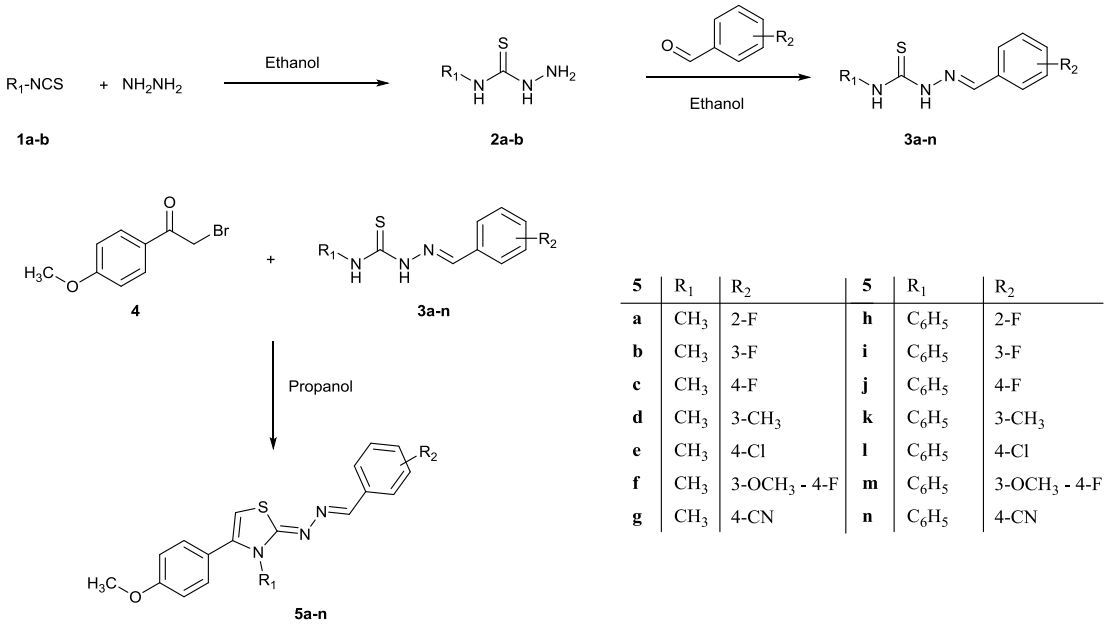

5	R_1	R_2	5	R_1	R_2
a	CH_3	2-F	**h**	C_6H_5	2-F
b	CH_3	3-F	**i**	C_6H_5	3-F
c	CH_3	4-F	**j**	C_6H_5	4-F
d	CH_3	3-CH_3	**k**	C_6H_5	3-CH_3
e	CH_3	4-Cl	**l**	C_6H_5	4-Cl
f	CH_3	3-OCH_3 - 4-F	**m**	C_6H_5	3-OCH_3 - 4-F
g	CH_3	4-CN	**n**	C_6H_5	4-CN

Scheme 1. Synthesis of targeted compounds **5a-n**.

Hydrazones **5a–n** could exist as couples of diastereoisomers E/Z. However, in each case only one isomer was detected by HPLC, ^{1}H and ^{13}C NMR analysis. Configuration of compounds could not be unambiguously assigned by NMR studies. However previous studies of the *E*/*Z* hydrazine interconversion reported in the literature indicates that the (*E*)-form dominates on the (*Z*)-form [28]. Moreover, several X-ray structures of such derivatives confirmed the (*E*)-stereochemistry adopted by 2-hydrazono-2,3-dihydro-1,3-thiazoles [29,30]. We could then assume that in this series, only the (*E*)-form was obtained. The proposed structures of all newly synthesized compounds were in full agreement with their elemental and spectral analyses, such as ^{1}H NMR, ^{13}C NMR and high-resolution mass spectrometry. ^{1}HNMR spectra for N-methyl substituted derivatives **5a-g** displayed significant broad singlet at δ 8.69-8.45 *ppm* for the benzylidene proton and a singlet peak for thiazolidine proton at δ 6.80-6.94 *ppm*, in addition to two characteristic singlet peaks at δ 3.82-3.83 and δ 3.82-3.83 *ppm* for phenyl methoxy group and N-methyl group, respectively. Also, compounds **5d** and **5f** showed an extra singlet peak at δ 3.91 *ppm* and δ 2.37 *ppm* for the benzylidene methoxy group for **5d** and benzylidene methyl group for **5f**, respectively. Similarly, the N-phenyl substituted derivatives **5h-n** displayed the same pattern of singlet peaks at δ 8.17-8.34 *ppm*, δ 6.69-6.80 *ppm* and δ 3.69 *ppm* for benzylidene proton, thiazolidine proton and phenyl methoxy group, respectively. On the other hand, compounds **5k** and **5m** showed an extra singlet peak at δ 3.88 *ppm* and δ 2.34 *ppm* for the benzylidene methoxy group for **5k** and benzylidene methyl group for **5m**, respectively.

^{13}CNMR spectra for all compounds showed peaks for the aromatic carbons, methoxy and methyl carbons at the expected values. Finally, the high-resolution mass spectrometry for all derivatives gave results within the difference range of 0.0001-0.001 from the calculated values.

2.3. Biological activity

2.3.1. In vitro single-dose cellular antiproliferative assay

All final synthesized compounds **5a-n** were tested for in vitro anticancer activity against 59 distinct human tumor cell lines (NCI panel), originating from nine different kinds of cancer, at a concentration of 10 μM (Table S1 and S2). To get a comprehensive idea about the efficacy of the new hydrazinothiazole series against the

59-cancer cell lines, the average of growth inhibition (GI) percentages obtained with compounds **5a-n** against each cell line was calculated, and the results are displayed in Fig. 3A. The results of the data analysis revealed that four cell lines were highly sensitive to these compounds (K-562 and SR leukemia, HCT-116 colon cancer and SK-MEL-5 melanoma cells), with an average of GI above 40% (Fig. 3.A, orange bars). This series of compounds was also active against eight other cell lines, with an average of GI between 30 and 40% (Fig. 3B, yellow bars). Then, the percentage of GI for each compound was determined against these twelve selected cell lines. The results are presented in Fig. 3B.

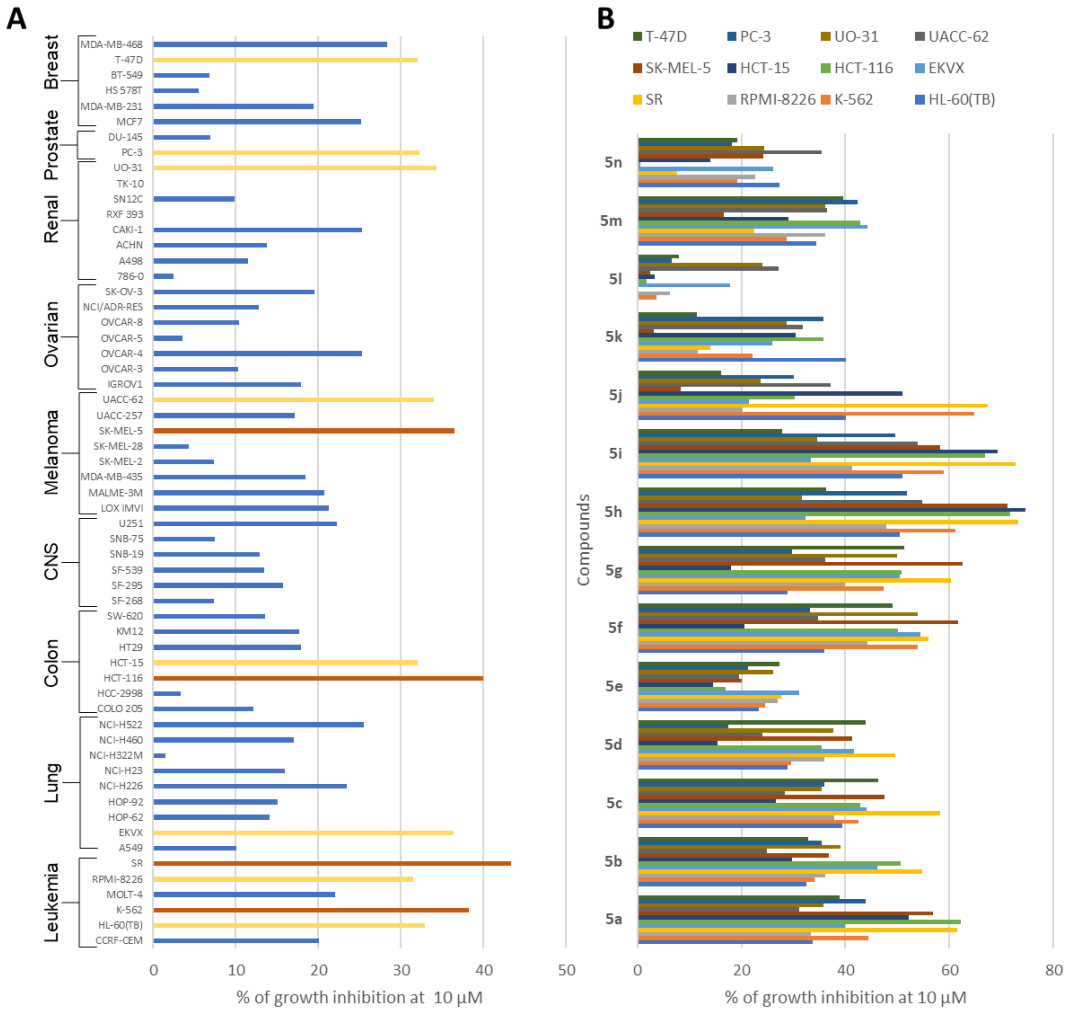

Fig. 3: A. Cell line sensitivity to compounds **5a-n**. The average of growth inhibition (GI) obtained with all compounds of the series was calculated for each cell line of the panel. Orange bars correspond to an average of GI above 40%, the yellow bars correspond to an average of GI between 30 and 40% and the blue bars, an average of

GI below 30%. **B**. GI percentage of the most sensitive cell lines after treatment with **5a-n** at a single dose of 10 µM.

In this study, we have synthesized two sub-series of compounds: one with a methyl moiety at position 3 of the dihydrothiazole ring (compounds **5a** to **5g**), and the other with a phenyl moiety at position 3 of the dihydrothiazole (compounds **5h** to **5n**). Structure–activity relationship was based on the obtained results by introducing different aryl substitution at the hydrazinylidene moiety.

In the *N*-methyl-2,3-dihydrothiazolidine series, compound **5a** with an *ortho*-fluorophenyl group was particularly active against SR leukemia cells (GI of 61.5%), HCT-116 and HCT-15 colon cancer cells (62.2% and 52.2%, respectively), and SK-MEL-5 melanoma cells (56.8%). Substitution with a *meta*-fluorophenyl group (compound **5b**) or with a *para*-fluorophenyl group (compound **5c**) led to a slight decrease of the GI percentage against these same cell lines. For example, the GI percentage against the HCT-116 cells decreased from 62.2% to 50.7%, to finally reached 42.8% for compound **5c**. The substitution of a *meta*-fluorine group by a *meta*-methyl group maintained the activity, compound **5d** being notably active against SR leukemia cells (GI of 49.6%), HCT-116 colon cancer cells (35.5%) and SK-MEL-5 melanoma cells (41.3%). On the other hand, substitution with a 4-chlorophenyl group dramatically decreased the activity in most cell lines; compound **5e** only showed moderate activity against EKVX non-small cell lung cancer cells with a GI of 31%. Substitution with a phenyl moiety bearing a fluorine atom at position 4 and a methoxy group at position 3 (compound **5f**) globally increased the activity. Thus, compared to compound **5c** only bearing a *para*-fluorine atom, compound **5f** was more active against K-562 leukemia cells (GI of 54%, compared to 42.6% for 5c), EKVX non-small cell lung cancer cells (54.4% compared to 44.1%) and SK-MEL-5 melanoma cells (61.6% compared to 47.6%). Furthermore, compound **5g** with a *para*-CN phenyl moiety demonstrated good GI activity, comparable to that obtained with compound **5a**. Thus, compound **5g** was particularly active against SR leukemia (GI of 60.3%) and SK-MEL-5 melanoma cells (62.5%).

In the second series bearing a phenyl group in the thiazolidine ring, compound **5h** with an *ortho*-fluorophenyl group markedly increased cell growth inhibition, compared to its methyl analog **5a**. Thus, compound **5h** showed GI above 50% against

17 cell lines of the NCI panel and this compound was particularly active against SR leukemia cells (GI of 73.2%), NCI-H460 non-small cell lung cancer cells (76.3%), HCT-116 and HCT-15 colon cancer cells (71.7% and 74.7%, respectively), LOX IMVI and SK-MEL-5 melanoma cells (71.8% and 71.2%, respectively). Substitution with a *meta*-fluorophenyl group also led to good results. Thus, compound **5i** demonstrated good cell GI against SR leukemia cells (72.8%), HCT-116 and HCT-15 colon cancer cells (66.9% and 69.3%, respectively). Moreover, as observed in the *N*-methyl-2,3-dihydrothiazole series, substitution with a *para*-fluorophenyl group (compound **5j**) led to a slight decrease of the activity, while a substitution with a 4-chlorophenyl group (compound **5l**) abolished the activity. Surprisingly, whereas the introduction of a 3-methoxy-4-flurophenyl or a 4-cyanophenyl group led to an increase of activity in the *N*-methyl-2,3-dihydrothiazole series, such substituents were not tolerated in the phenyl-thiazolidine series, compounds **5m** and **5n** being only weakly active.

2.2.2. In vitro cytotoxicity against HCT-116

To confirm the potential anti-proliferative activity of the 2-hydrazino-2,3-dihydrothiazole derivatives, dose-response experiments were carried out against the HCT-116 colon cancer cell line, using the sulforhodamine B colorimetric assay [35]. Doxorubicin was used as a reference drug in the experiment. IC_{50} values have been determined and are shown in Table 1. Compounds **5a**, **5h-i** and **5n** showed good cytotoxic activity, similar to Doxorubicin with an IC_{50} between 6.9 and 11.2 µM. As previously observed with the single-dose assay, an *ortho*-fluorophenyl group was preferred in the *N*-methyl-2,3-dihydrothiazole series, compound **5a** being the most active of this first series. Concerning the phenyl-thiazolidine derivatives, the presence of a *meta*-fluorophenyl group led to the best potency (compound **5i**, IC_{50} of 6.9 µM), followed by the *para*-cyanophenyl and the *ortho*-fluorophenyl derivatives (compounds **5n** and **5h**, IC_{50} of 10.8 and 11.2 µM respectively).

Compound	IC_{50} HCT-116 (µM)[a]
5a	10.9 ± 0.013
5b	40.8 ± 0.016
5c	20.7 ± 0.023
5d	38.4 ± 0.014
5e	24.0 ± .006
5f	12.7 ± 0.008
5g	24.8 ± 0.007
5h	11.2 ± 0.004
5i	6.9 ± 0.013
5j	12.4 ± 0.034
5k	40.5 ± 0.019
5l	34.9 ± 0.018
5m	31.2 ± 0.007
5n	10.8 ± 0.013
Doxorubicin	11.2 ± 0.011

[a] IC_{50} values are the mean ± S.D. of three separate experiments.

Table 1. Cytotoxicity of compounds **5a-n** (IC_{50}) against HCT-116 cells.

Then, the most active compound of each series (methyl- or phenyldihydro-thiazole), namely compounds **5a** and **5i**, were selected and their cytotoxic activity was determined on the normal fibroblast cell line WI-38 (Table 2). The two compounds showed weak cytotoxicity against these cells, with an IC_{50} of 73.5 µM and 90.1 µM, representing a selectivity index (SI) of 6.7 to 13.1 respectively, compared to IC_{50} values against HCT-116 cancer cells. These results showed that some of these new 2-hydrazino-2,3-dihydrothiazole derivatives are very optimistic candidates as relatively safe cytotoxic agents. Consequently, the most potent analogs were subjected to further investigations concerning their potential anti-proliferative mechanism of action.

Compound	IC_{50} HCT-116 (µM)[a]	IC_{50} WI-38 (µM) [a]	SI
5a	10.9 ± 0.013	73.5 ± 0.009	6.7
5i	6.9 ± 0.013	90.1 ± 0.01	13.1

[a] IC_{50} values are the mean ± S.D. of three separate experiments.

Table 2. Effect and selectivity index of compounds **5a** and **5i** against WI-38 normal cells.

2.3.3 In vitro EGFR inhibition activity:

A further EGFR kinase test was performed against HCT-116 cell line, which are known for their EGFR overexpression, to investigate the proposed mechanism of action of the newly synthesized compounds. Compounds **5a**, **5f**, **5h-j** and **5n**, that showed the best cytotoxic effect against the HCT-116 cell line, were chosen for further investigation into their *in vitro* EGFR inhibitory activities (Table 3). All tested compounds showed good inhibitory activity with IC_{50} range between 0.215 and 0.524 µM, only slightly less potent than the clinically used kinase inhibitor Erlotinib, which exhibited an IC_{50} value of 0.136 µM. In these series, compound **5i** displayed the higher potency (IC_{50} of 0.215 µM), followed by compound **5a** (IC_{50} of 0.253 µM). Compounds **5f**, **5h**, **5j** and **5n** exhibited the least inhibitory activity of these series, with IC_{50} values ranged from 0.395 to 0.524 µM. Moreover, the results showed that the EGFR inhibitory activities matched perfectly with the cytotoxic activities of compounds **5a** and **5i**, implying that the anti-proliferative effect might be due to EGFR enzyme inhibition.

Compound	EGFR IC_{50} (µM)[a]
5a	0.253±0.004
5f	0.524±0.009
5h	0.468±0.005
5i	0.215±0.003
5j	0.395±0.003
5n	0.416±0.007
Erlotinib	0.136±0.002

[a] IC_{50} values are the mean ± S.D. of three separate experiments.

Table 3. IC_{50} values against EGFR.

2.2.4. Cell cycle distribution analysis

The most potent compounds (**5a** and **5i)** were chosen to further investigate their cellular mechanism of action. HCT-116 cells were treated with DMSO (control) or compound **5a** and **5i** and the DNA content was analyzed by flow cytometry. The results are presented in Figure 4. Both compounds appeared to exhibit similar patterns of cell-cycle arrest. An increase in the subG1 phase was observed for cells treated by compounds **5a** and **5i** (17.61% and 21.62%, respectively), compared to 3.11% in control. Moreover, the percentage of cells in the G2/M phase of the cell cycle rose from 21.35% for untreated HCT-116 cells to 35.19% and 29.24% for compounds **5a**

and **5i**, respectively. These results suggest that compounds **5a** and **5i** obviously interfered with the G2-to-M phase transition and promoted the entry of cells into subG1, the apoptotic phase.

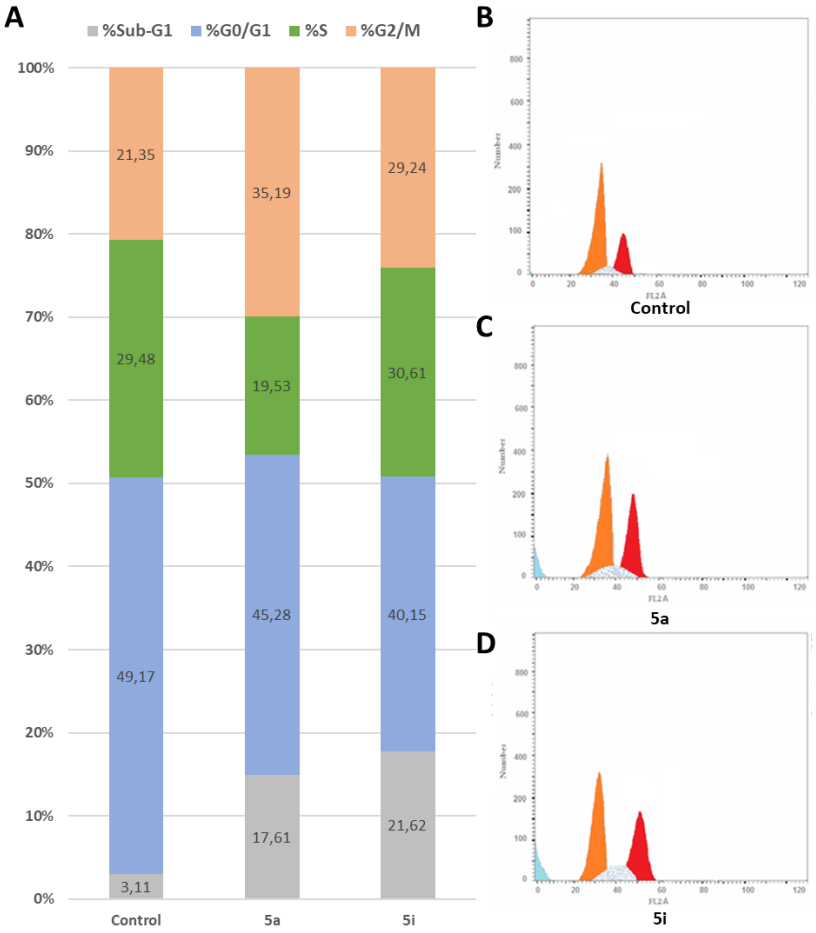

Fig. 4: Cell distribution (**A**) in the subG1, G0/G1, S and G2/M phases for HCT-116 cells after treatment with control (**B),** compounds **5a** (**C**) and **5i** (**D**).

2.2.4. Apoptosis assay

The Annexin V-FITC/PI double staining (AV/PI) apoptosis test was performed to assess whether the growth suppression activity of compounds **5a** and **5i** is congruent with the induction of apoptosis proposed by the increasing population of sub-G1 in the treated HCT-116 cells. Figure 5 depicted the findings of this test, which demonstrated that compounds **5a** and **5i** triggered both early and late apoptosis in HCT-116 cell lines. Indeed, the percentage of total apoptotic cells increased from 1.91% of early apoptosis and 1.27% of late apoptosis in untreated HCT-116 cells to 7.18% of early apoptosis and 9.11% of late apoptosis in HCT-116 treated with

compound **5a**, and from 6.47% of early apoptosis and 13.46% of late apoptosis in HCT-116 cells treated with compound **5i**. These results showed that compounds **5a** and **5i** were able to increase in total apoptosis of HCT-116 cells with an approximately 3.9-folds and 4.8-folds respectively, compared to the control.

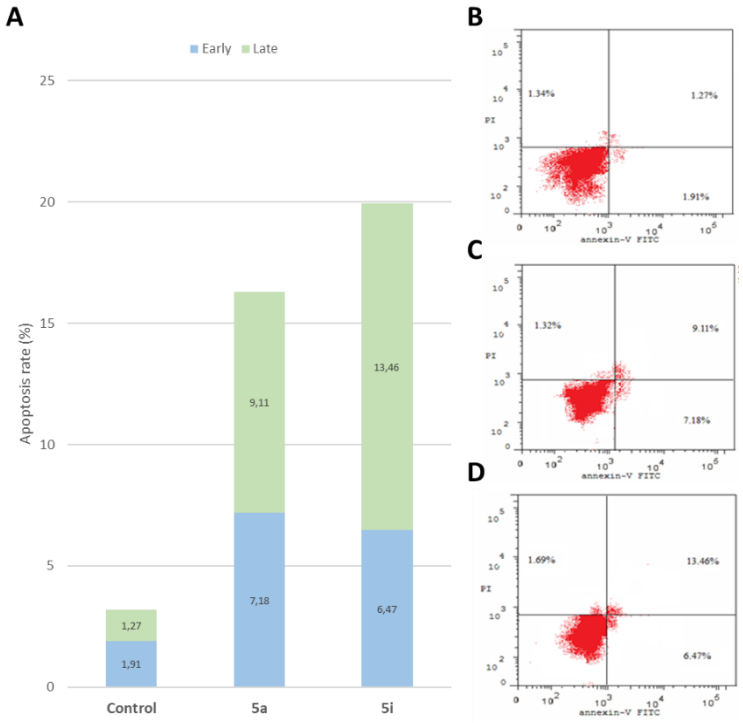

Fig. 5: Quantification of apoptosis rate (%) in flow cytometry (**A**). Effect of control (**B**), compounds **5a** (**C**) and **5i** (**D**) on the percentage of annexin V-FITC-positive staining in HCT-116 cells.

2.2.5. Effect of compounds 5a and 5i on Bcl-2 and Bax levels.

The Bcl-2 family, the best-studied protein family implicated in apoptosis control, is consisting of both anti-apoptotic and pro-apoptotic members [28]. Anti-apoptotic members, such as Bcl-2, inhibits apoptosis, whereas pro-apoptotic members of the Bcl-2 family, such as Bax, stimulates cytochrome c release, caspase activation and apoptosis [31]. As a result, the Bcl-2 protein family stands as a critical decision point between life and death in the common pathway of apoptosis.

To confirm the role of compounds **5a** and **5i** on apoptosis, the expression of the Bax and Bcl-2 proteins was studied and compared to untreated HCT-116 cells. As shown in Figure 6, compounds **5a** and **5i** enhanced the Bax level and significantly lowered the Bcl-2 level, compared with control. These results suggested ability of compounds **5a** and **5i** to suppress BCL-2 gene expression and thereby promoted

cancer cell death. Furthermore, compounds **5a** and **5i** induced Bax protein expression that positively correlates with apoptosis.

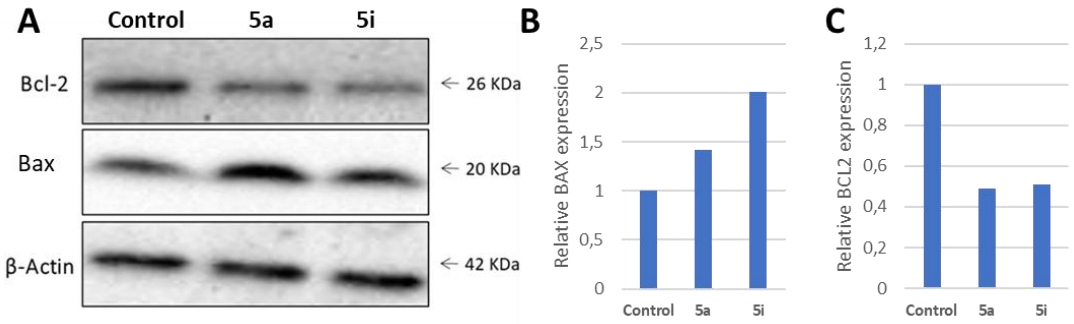

Fig. 6: Effect of compounds **5a** and **5i** on the expression of Bcl-2 and Bax proteins in HCT-116 cell line. **A**. HCT-116 cells were treated with 10.9 µM of compound **5a** and 6.9 µM of compound **5i** and anti-apoptotic marker Bcl-2 expressions and apoptotic marker Bax was determined using western blot. Actin was utilized as a loading control in all these analyses. The data are normalized to β-actin, and the values are given as fold changes from the control, which is set to "1.0" (**B** and **C**).

2.3. Modeling Studies

2.3.1. Docking study

Molecular docking simulations were performed considering only the derivatives which were active against HCT116 cell line and inhibited EGFR. Validation of the docking protocol was carried out using Erlotinib complexed to EGFR (PDB code: 1M17) and Molecular operating environment (MOE 2019.02) Software [30]. After optimization of hydrogens and charges of the receptor, redocking of the inhibitor showed a root-mean-square deviation (RMSD) value of 0.85 Å, predicting co-crystallized binding pose correctly. After that, all the synthesized compounds were then docked into the EGFR-binding domain.

Inspecting the 2D interaction diagram between Erlotinib and EGFR revealed that this inhibitor interacts via the N1 of the quinazoline ring through H-bonds with the Met769 amide NH, the other quinazoline nitrogen (N3) interacted with a water molecule present in the active site of the kinase (Fig. 7). Several other interactions, including Glu738, Leu768 and Leu 694 were also involved in the binding of Erlotinib into the ATP active site of EGFR [31].

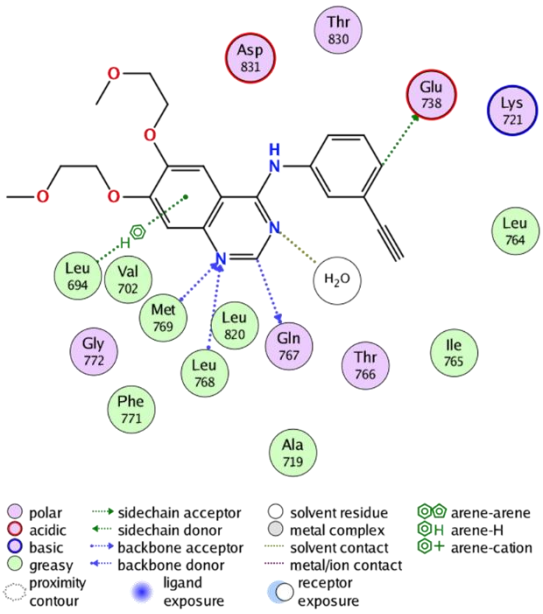

Fig. 7: Molecular interactions of Erlotinib at the EGFR tyrosine kinase domain active site (PDB code: 1M17). Ligand is colored by element type (C, grey; N, blue; O, red; S, yellow; F, green); key bonds are shown by dashed lines connecting the atoms.

Interestingly, the docking of all the newly synthesized compounds induced a favorable binding with EGFR, as evidenced by their excellent docking scores ranging from -10.2 to -12.1 Kcal/Mol. Focusing on compounds **5a** and **5i**, both were able to achieve binding pattern very similar to that of Erlotinib, as expected when designing this series of compounds**.** The synthesized compounds **5a** and **5i** achieved docking scores of -11.6 and -12.1 Kcal/mole respectively, that nearly match the docking score of Erlotinib (-12.4 Kcal/mole). As depicted from Figures 8A and 8B, the *N*-methyl dihydrothiazole ring in compound **5a** involved in four interactions with the key residues of EGFR, three hydrogen bonds with Gln767 and Met769 and one hydrophobic interaction with Leu768. In addition, the *para*-methoxy-phenyl ring was engaged in two hydrophobic interactions with Leu694 and Gly772. Moreover, the *ortho*-fluoride substituent formed a hydrogen bond interaction with Lys721.

In a similar manner, compound **5i** was engaged in six interactions with the key residues of EGFR, four hydrogen bonds with Thr766, Gln767and Met769 and two hydrophobic bonds with Leu768 and Leu694 via its *N*-phenyl-2,3-dihydrothiazole ring. Also, the *para*-methoxy-phenyl ring of compound **5i** was engaged in two hydrophobic interactions with Leu694 and Gly772, while the *meta*-fluoride substituent formed a hydrogen bond interaction with Lys721. The superiority of

compound **5i** over compound **5a** in both docking score and biological activity is attributed to the ability of its *N*-phenyl-2,3-dihydrothiazole ring to form multiple interactions with EGFR key residues. This is due to the large size of the phenyl ring that forces the dihydrothiazole ring toward the key residues Thr766, Leu694, Gln767, Met769 and Leu768 (Figures 8C and 6D).

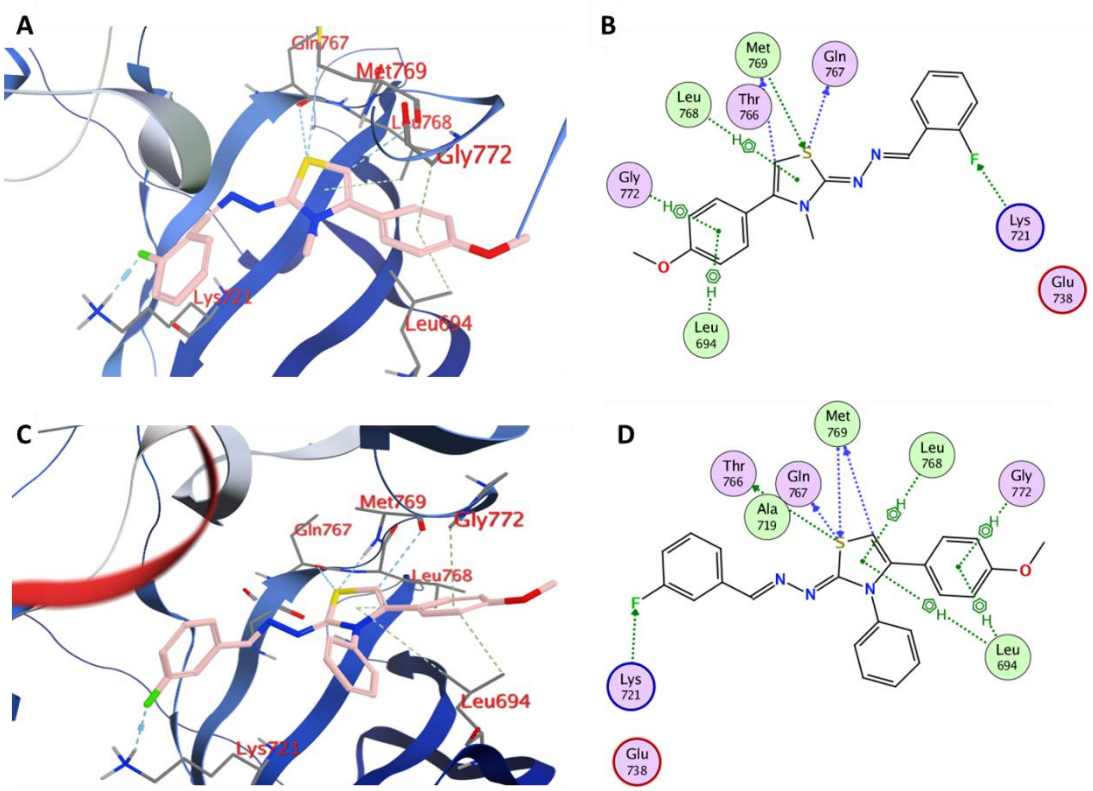

Fig. 8: Molecular interactions of compound **5a** (**A** and **B**) and compound **5i** (**C** and **D**) at the EGFR tyrosine kinase domain active site. **A** and **C**: Key interactions of **5a** (**A**) and **5i** (**C**) into the active site of EGFR. The enzyme is represented as cartoon mode and the compounds are shown as pink stick representation. Key bonding interactions are indicated as dotted lines. **B** and **D**: Ligand is colored by element type (C, grey; N, blue; O, red; S, yellow; F, green), key bonds are shown by dashed lines connecting the atoms (see Fig.7 caption for the color code).

2.3.2. Molecular Dynamics

Further virtual investigations were achieved by molecular dynamic (MD) simulations studies. MD simulation provides several valuable parameters to investigate the dynamicity of biological complexes. Also, MD studies could give insights into accurate speculation of the binding affinity and intensity of docked complexes of a ligand and target proteins. Consequently, the binding coordinates revealed from the docking of EGFR with compounds **5a** and **5i** were moved forward to MD simulation.

To provide a comparative mean for the effect of each ligand on the stability of the EGFR enzyme, the later was subjected to MDS in its Apo form in addition to the X-ray coordinates of EGFR-Erlotinib complex. Four MD simulations were conducted for 150ns using GROMACS 5.1.1 software [32]. As illustrated in Figure 9, the two proposed inhibitors had the prerogative of stabilizing the dynamic EGFR enzyme, as indicated by their lower RMSD values in comparison to the RMSD value of Apo EGFR and nearly matches that of Erlotinib. Indeed, the EGFR-Erlotinib**,** EGFR-**5a** and EGFR-**5i** complexes had RMSD values of 1.35, 1.85 and 1.41 Å, respectively, while the RMSD of the Apo EGFR reached 4.12 Å (Figure 9A). Thus, the ability of compounds **5a** and **5i** to limit the dynamic nature of the EGFR via formation of stable complexes, as indicated by the lower RMSD values, is a valid indicator on their inhibitory effect on EGFR. Similar results to the RMSD values were obtained in the analysis of root mean square deviation (RMSF) and radius of gyration (RG). As expected, EGFR-Erlotinib, EGFR-**5a** and EGFR-**5i** complexes had an average RMSF values of 1.71, 1.87 and 1.75 Å, respectively for all the residues, while the RMSD of the Apo EGFR reached 3.53 Å (Figure 9B). Besides, the Radius results showed higher gyration of the Apo EGFR form reaching RG value of 17.2 Å, in comparison, EGFR-Erlotinib**,** EGFR-**5a** and EGFR-**5i** had lesser RG values of 8.5, 10.1, 12.3 Å, respectively (Figure 9C).

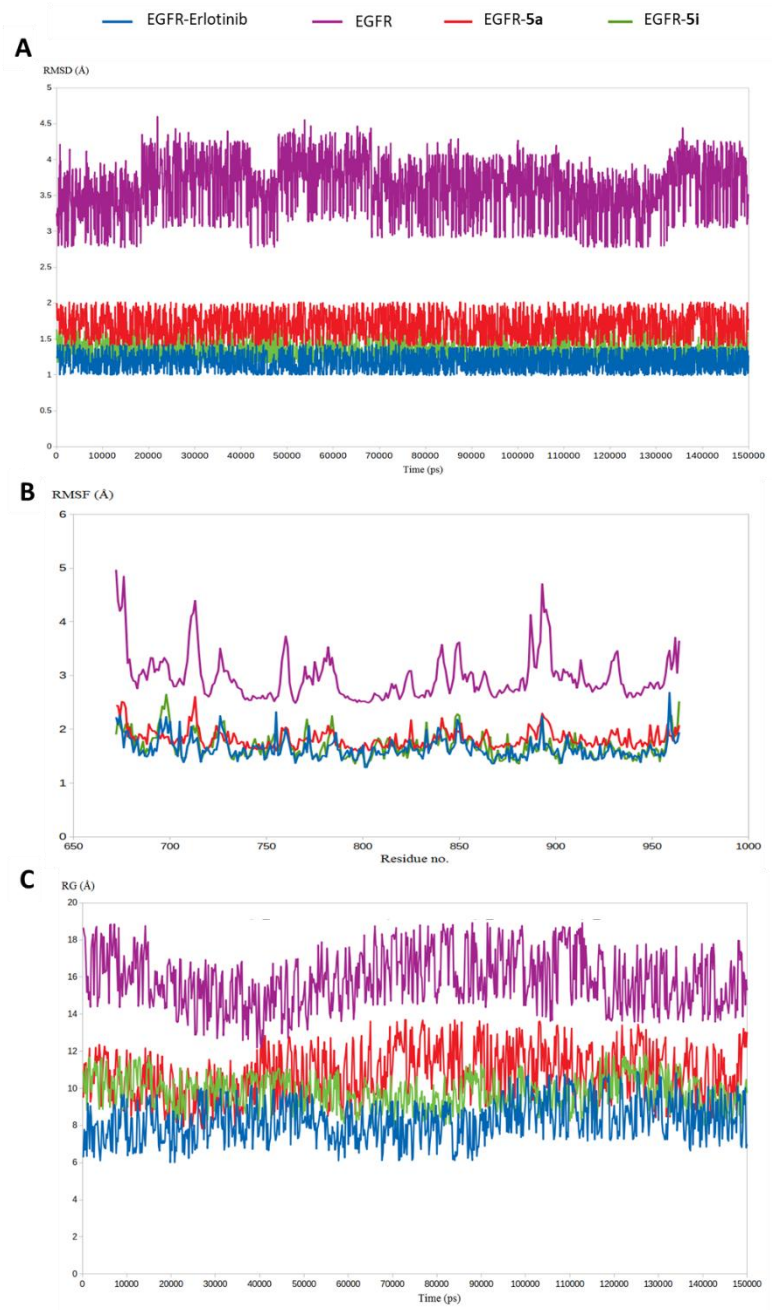

Fig. 9: MD simulations. **A**: RMSD analysis; **B**. RMSF analysis; **C**. RG analysis.

2.3.3. Binding Free Energy Calculations using MM-PBSA approach

For further validation of the binding intensity between the newly developed compounds **5a** and **5i** and the EGFR enzyme, the MM-PBSA package [33] was brought in action to evaluate the binding free energies between compounds **5a** and **5i** and EGFR enzyme. The produced trajectories from the production stage were utilized to count all the forms of binding free energy. Different types of energy including Van

der Waals energy, Electrostatic energy, Polar solvation energy and SASA energy were calculated for the two complexes containing EGFR bound to **5a** or **5i** (Table 4).

Table 4. The binding free energies of compounds **5a**, **5i** and Erlotinib in complex with EGFR.

Complex	**$\Delta E_{binding}$** (kJ/mol)	**$\Delta E_{Van\ der\ Waals}$** (kJ/mol)	**$\Delta E_{Electrostatic}$** (kJ/mol)	**$\Delta E_{polar\ solvatation}$** (kJ/mol)	**SASA** (kJ/mol)
5a	-266.7± 4.0	-201.5± 5.8	-109.7±4.1	75.3± 1.6	-30.8± 0.2
5i	-295.9± 3.9	-226.9± 5.7	-118.4±3.6	81.3± 2.1	-31.9± 0.3
Erlotinib	-300.9± 4.1	-231.4± 5.9	-114.9±3.8	78.7± 2.2	-33.3± 0.2

The calculated binding free energy for the two compounds were comparable to each other, in which compound **5a** and **5i** achieved binding free energies of -266.7 ± 4.0 and -295.9 ± 3.9 (kJ/mol) respectively. Interestingly, the calculated binding free energies for the two compounds were very close to that of Erlotinib that achieved -300.9± 4.1 (kJ/mol). These results boosted all the in-silico calculations supporting the prognosticated binding mode of both **5a** and **5i** within EGFR. Moreover, all the MD and energy calculations favored compound **5i** over compound **5a**, as consistent with the early results of enzyme assay.

3. Conclusions

In this study, we reported the use of the 2-hydrazino-2,3-dihydrothiazole moiety as the pharmacophore to access new EGFR inhibitors. Based on the key interaction elements of Erlotinib with EGFR, a series of 14 compounds were designed and synthesized. All compounds were evaluated on the NCI-60 cell line panel at a 10 µM single dose. K-562 and SR leukemia, HCT-116 colon cancer and SK-MEL-5 melanoma cells appeared to be particularly sensitive to these compounds, with an average of growth inhibition above 40%. Among the studied modulations, the introduction of a phenyl group on the dihydrothiazole moiety increased the activity, as well as an *ortho*- or *meta*-fluorophenyl group at the hydrazinylidene moiety. IC_{50} was then determined, using the HCT-116 colon cancer cell line. Regarding the two sub-

series studied (*N*-methyl- or *N*-phenyldihydrothiazole), compounds **5a** and **5i** revealed to be the most potent compounds in each sub-series, with an IC_{50} of 6.9 ± 0.013 µM and 10.9 ± 0.013 µM. These two compounds were relatively safe towards normal human fibroblasts (WI-38), representing a selectivity index of 6.7 and 13.1, respectively. Moreover, these two compounds showed the best potency to inhibit the EGFR, with an IC_{50} of 215 ± 3 nM and 253 ± 4 nM, relatively similar to Erlotinib (IC_{50} of 136 ± 2 nM). Further mechanistic studies showed that compounds **5a** and **5i** interfered with the G2-to-M phase transition, enhanced the expression of the pro-apoptotic Bax protein and lowered the pre-apoptotic bcl-2 protein levels, which thereby promoted apoptosis of HCT-116 cells. Finally, docking studies revealed that compounds **5a** and **5i** were positioned in a very similar manner to Erlotinib into the EGFR active site. More detailed analyses, using docking, molecular dynamics and binding free energy calculations confirmed that compound **5i** is a potent EGFR inhibitor. Thus, all these results suggested that the use of a 2-hydrazino-2,3-dihydrothiazole moiety as a pharmacophore is a valuable strategy to design new EGFR inhibitors.

4. Experimental

4.1. Chemistry

Melting points (°C) of the synthesized compounds were measured using Electrothermal Stuart 5MP3 and were uncorrected. Following up of reactions was conducted using silica gel 60 F254 - TLC plates (Merck). The NMR analyses had been measured using Bruker-Avance 400 NMR spectrometer (400 MHz for ^{1}HNMR and 101 MHz for ^{13}CNMR) and Bruker-Avance 500 NMR spectrometer (500 MHz for ^{1}HNMR and 126 MHz for ^{13}CNMR) in deuterated dimethylsulfoxide (DMSO-*d6*). Chemical shifts (δ_H) were reported relative to the solvent (DMSO-d_6). LC/MS analyses were recorded on a Quattro microTM ESI triple quadrupole mass spectrometer (ESI+ electrospray ionisation mode) coupled to an Alliance HPLC system (Waters, Milford, USA) equipped with a Chromolith High Resolution RP-18e column (25 x 4.6 mm), with the samples being previously separated using a gradient from 100% (H_2O + 0.1% HCO_2H) to 100% (ACN + 0.1% HCO_2H) in 3 min at a flow rate of 3 mL/min and with UV detection at 214 nm. High Resolution Mass

Spectrometry (HRMS) analyses were performed with a time-of-flight (TOF) spectrometer coupled to a positive electrospray ionization (ESI) source, at the Laboratoire de Mesures Physiques, University of Montpellier, France. Elemental analyses were measured at Al-Azhar University, Cairo, Egypt.

4.1.1. General method for synthesis of compounds 5a-n

An equimolar amount of respective thiosemicarbazide **2a-b** (2 mmol) and appropriate aromatic aldehyde were heated in 25 mL of ethanol under reflux for 5 hours, in the presence of a catalytic amount of HCl. After cooling, the solid was filtered and crystallized from ethanol to afford the corresponding aryl-thiosemicarbazone **3a-n,** which was then engaged in the following step without additional purification. Compounds **3a-n** (1 mmol) were then reacted with 2-bromo-1-(4-methoxyphenyl)ethan-1-one in 25 mL of propan-2-ol and the reaction mixture refluxed for 2 h. Upon cooling, the resulting solid was filtered and then crystallized from proper solvent to afford the final compounds **5a-n**.

4.1.1.1. (Z)-2-(((E)-2-fluorobenzylidene)hydrazinylidene)-4-(4-methoxyphenyl)-3-methyl-2,3-dihydrothiazole (5a):

Brownish powder (yield 60%); m.p. 216-218 ^{o}C; ^{1}H NMR: δ 8.69 (br. s., 1H), 7.92 (t, *J* = 7.17 Hz, 1H), 7.50 - 7.58 (m, 1H), 7.48 (d, *J* = 8.54 Hz, 2H), 7.30 - 7.37 (m, 2H), 7.10 (d, *J* = 8.85 Hz, 2H), 6.94 (br. s., 1H), 3.82 (s, 3H), 3.49 (s, 3H). ^{13}C NMR: δ 169.0, 161.7, 160.4, 159.7, 143.4, 141.8, 132.6, 130.8, 126.7, 125.1, 121.0, 116.3, 114.4, 104.3, 55.4, 35.2. MS (ESI) m/z: 342 $[M+H]^{+}$; HRMS (ESI) m/z $[M+H]^{+}$: Calcd. 342.1071, Found, 342.1078; Anal. Calcd. for $C_{18}H_{16}FN_3OS$ (341.40); % C, 63.33; H, 4.27; N, 12.31, Found: % C, 63.50; H, 4.81; N, 12.49.

4.1.1.2. (Z)-2-(((E)-3-fluorobenzylidene)hydrazinylidene)-4-(4-methoxyphenyl)-3-methyl-2,3-dihydrothiazole (5b):

Buff powder (yield 65%); m.p. 211-213 ^{o}C; ^{1}H NMR: δ 8.45 (s, 1H), 7.58 - 7.64 (m, 1H), 7.55 (t, *J* = 8.56 Hz, 2H), 7.47 (d, *J* = 8.56 Hz, 2H), 7.29 (t, *J* = 7.58 Hz, 1H), 7.08 (d, *J* = 8.31 Hz, 2H), 6.80 (s, 1H), 3.82 (s, 3H, masked by water peak), 3.44 (s, 3H). ^{13}C NMR: δ 161.3, 160.4, 155.5, 149.3, 141.6, 139.3, 131.7, 130.8, 123.6,

120.5, 114.5, 112.9, 109.1, 102.9, 55.5, 34.4. MS (ESI) m/z: 342 $[M+H]^+$; HRMS (ESI) m/z $[M+H]^+$: Calcd. 342.1071, Found, 342.1077; Anal. Calcd. for $C_{18}H_{16}FN_3OS$ (341.40); % C, 63.32; H, 4.27; N, 12.31, Found: % C, 63.54; H, 4.90; N, 12.54.

4.1.1.3. (Z)-2-(((E)-4-fluorobenzylidene)hydrazinylidene)-4-(4-methoxyphenyl)-3-methyl-2,3-dihydrothiazole (5c):

Brownish powder (yield 72%); m.p. 250-251 ^oC; ^1H NMR: δ 8.46 (br. s., 1H), 7.80 - 7.87 (m, 2H), 7.47 (d, *J* = 8.54 Hz, 2H), 7.30 - 7.37 (m, 2H), 7.09 (d, *J* = 8.70 Hz, 2H), 6.80 (br. s., 1H), 3.83 (s, 3H), 3.43 (br. s., 3H). ^{13}C NMR: δ 168.8, 164.2, 162.3, 160.3, 149.3, 141.5, 130.6, 129.3, 121.3, 116.0, 114.3, 102.9, 55.3, 34.6. MS (ESI) m/z: 342 $[M+H]^+$; HRMS (ESI) m/z $[M+H]^+$: Calcd. 342.1071, Found, 342.1074; Anal. Calcd. for $C_{18}H_{16}FN_3OS$ (341.40); % C, 63.32; H, 4.27; N, 12.31, Found: % C, 63.59; H, 4.86; N, 12.57.

4.1.1.4. (Z)-4-(4-methoxyphenyl)-3-methyl-2-(((E)-3-methylbenzylidene) hydrazinylidene)-2,3-dihydrothiazole (5d):

Buff powder (yield 62%); m.p. 222-224 ^oC; ^1H NMR: δ 8.48 (s, 1H), 7.58 (s, 1H), 7.48 (d, *J* = 8.68 Hz, 2H), 7.42 (d, *J* = 8.68 Hz, 1H), 7.35 - 7.39 (m, 1H), 7.28 - 7.32 (m, 1H), 7.10 (d, *J* = 8.68 Hz, 2H), 6.91 (s, 1H), 3.83 (s, 3H), 3.48 (s, 3H), 2.37 (s, 3H). MS (ESI) m/z: 338 $[M+H]^+$; HRMS (ESI) m/z: Calcd. 338.1322, Found, 338.1332; Anal. Calcd. for $C_{19}H_{19}N_3OS$ (337.44); % C, 67.63; H, 5.68; N, 12.45, Found: % C, 67.41; H, 5.82; N, 12.71.

4.1.1.5. (Z)-2-(((E)-4-chlorobenzylidene)hydrazinylidene)-4-(4-methoxyphenyl)-3-methyl-2,3-dihydrothiazole (5e):

Buff powder (yield 77%); m.p. 250-252 ^oC; ^1H NMR NMR: δ 8.48 (s, 1H), 7.8 (d, *J* = 7.78 Hz, 2H), 7.5 (d, *J* = 7.32 Hz, 2H), 7.47 (d, *J* = 8.39 Hz, 2H), 7.09 (d, *J* = 8.54 Hz, 2H), 6.85 (br. s., 1H), 3.82 (s, 3H), 3.46 (s, 3H). ^{13}C NMR: δ 169.6, 168.3, 160.8, 150.5, 149.7, 132.0, 131.2, 129.5, 129.2, 121.9, 114.8, 103.4, 55.9, 35.1. MS (ESI) m/z: 358 $[M+H]^+$; HRMS (ESI) m/z $[M+H]^+$: Calcd. 358.0775, Found,

358.0779; Anal. Calcd. for $C_{18}H_{16}ClN_3OS$ (357.86); % C, 60.41; H, 4.51; N, 11.74, Found: % C, 60.63; H, 4.69; N, 11.86.

4.1.1.6. (Z)-2-(((E)-4-fluoro-3-methoxybenzylidene)hydrazinylidene)-4-(4-methoxyphenyl)-3-methyl-2,3-dihydrothiazole (5f):

Brownish powder (yield 81%); m.p. 227-228 ^oC; ^1H NMR: δ 8.49 (s, 1H), 7.54 (d, *J* = 7.02 Hz, 1H), 7.48 (d, *J* = 8.54 Hz, 2H), 7.31 - 7.40 (m, 2H), 7.10 (d, *J* = 8.85 Hz, 2H), 6.93 (br. s., 1H), 3.91 (s, 3H), 3.83 (s, 3H), 3.49 (s, 3H). ^{13}C NMR: δ 168.7, 160.4, 154.0, 152.0, 149.5, 147.5, 141.8, 130.8, 121.0, 120.7, 116.4, 114.4, 111.8, 104.3, 56.0, 55.4, 35.2. MS (ESI) m/z: 372 $[M+H]^+$; HRMS (ESI) m/z $[M+H]^+$: Calcd. 372.1177, Found, 372.1180; Anal. Calcd. for $C_{19}H_{18}FN_3O_2S$ (371.43); % C, 61.44; H, 4.88; N, 11.31, Found: % C, 61.70; H, 4.97; N, 11.48.

4.1.1.7. 4-((E)-(((Z)-4-(4-methoxyphenyl)-3-methylthiazol-2(3H)-ylidene) hydrazinylidene) methyl)benzonitrile (5g):

Brownish powder (yield 76%); m.p. 245-247 ^oC; ^1H NMR: δ 8.49 (s, 1H), 7.79 (d, *J* = 7.78 Hz, 2H), 7.56 (d, *J* = 7.32 Hz, 2H), 7.48 (d, *J* = 8.39 Hz, 2H), 7.10 (d, *J* = 8.54 Hz, 2H), 6.86 (br. s., 1H), 3.83 (s, 3H), 3.47 (s, 3H). ^{13}C NMR: δ 169.1, 167.7, 160.2, 149.9, 149.1, 131.5, 130.6, 128.9, 128.7, 128.5, 121.4, 114.3, 102.9, 55.3, 34.6. MS (ESI) m/z: 349 $[M+H]^+$; HRMS (ESI) m/z: Calcd. 349.1118, Found, 349.1119; Anal. Calcd. for $C_{19}H_{16}N_4OS$ (348.42); % C, 65.50; H, 4.63; N, 16.08, Found: % C, 65.32; H, 4.81; N, 16.27.

4.1.1.8. (Z)-2-(((E)-2-fluorobenzylidene)hydrazinylidene)-4-(4-methoxyphenyl)-3-phenyl-2,3-dihydrothiazole (5h):

Yellowish powder (yield 72%); m.p. 259-260 ^oC; ^1H NMR: δ 8.34 (br. s., 1H), 7.90 (t, *J* = 8.16 Hz, 1H), 7.24 - 7.48 (m, 9H), 7.10 (d, *J* = 8.70 Hz, 2H), 6.80 (d, *J* = 8.70 Hz, 2H), 3.69 (s, 3H). ^{13}C NMR: δ 171.3, 169.3, 162.0, 159.9, 144.4, 140.6, 137.2, 132.1, 130.5, 129.7, 129.2, 127.2, 125.3, 122.9, 116.6, 116.4, 114.2, 102.5, 55.6. MS (ESI) m/z: 404 $[M+H]^+$; HRMS (ESI) m/z $[M+H]^+$: Calcd. 404.1227, Found, 404.1234; Anal. Calcd. for $C_{23}H_{18}FN_3OS$ (403.47); % C, 68.47; H, 4.50; N, 10.41, Found: % C, 68.59; H, 4.73; N, 10.58.

4.1.1.9. (Z)-2-(((E)-3-fluorobenzylidene)hydrazinylidene)-4-(4-methoxyphenyl)-3-phenyl-2,3-dihydrothiazole (5i):

Yellowish powder (yield 75%); m.p. 255-257 ^{o}C; ^{1}H NMR: δ 8.23 (s, 1H), 7.51 - 7.55 (m, 1H), 7.47 (dt, *J* = 5.72, 7.82 Hz, 2H), 7.37 - 7.44 (m, 2H), 7.34 - 7.36 (m, 1H), 7.27 - 7.32 (m, 1H), 7.24 (d, *J* = 7.32 Hz, 1H), 7.18 - 7.22 (m, 1H), 7.10 (d, *J* = 8.85 Hz, 2H), 6.73 - 6.86 (m, 3H), 3.69 (s, 3H). ^{13}C NMR: δ 163.3, 161.4, 159.4, 150.0, 140.2, 137.4, 136.6, 131.6, 130.1, 129.3, 128.8, 123.3, 122.3, 120.8, 116.7, 113.7, 112.9, 104.5, 55.2. MS (ESI) m/z: 404 $[M+H]^{+}$; HRMS (ESI) m/z $[M+H]^{+}$: Calcd. 404.1227, Found, 404.1229; Anal. Calcd. for $C_{23}H_{18}FN_3OS$ (403.47); % C, 68.47; H, 4.50; N, 10.41, Found: % C, 68.61; H, 4.62; N, 10.64.

4.1.1.10. (Z)-2-(((E)-4-fluorobenzylidene)hydrazinylidene)-4-(4-methoxyphenyl)-3-phenyl-2,3-dihydrothiazole (5j):

Buff powder (yield 66%); m.p. 235-237 ^{o}C; ^{1}H NMR: δ 8.23 (s, 1H), 7.75 (dd, *J* = 5.72, 8.77 Hz, 2H), 7.39 - 7.45 (m, 2H), 7.32 - 7.39 (m, 3H), 7.28 (t, *J* = 8.85 Hz, 2H), 7.08 - 7.12 (m, *J* = 8.70 Hz, 2H), 6.77 - 6.82 (m, *J* = 8.70 Hz, 2H), 6.73 (s, 1H), 3.69 (s, 3H). ^{13}C NMR: δ 164.5, 162.5, 159.9, 150.8, 140.5, 137.3, 132.1, 130.5, 129.6, 129.2, 129.0, 123.0, 116.4, 116.2, 114.2, 102.1, 55.6. MS (ESI) m/z: 404 $[M+H]^{+}$; HRMS (ESI) m/z $[M+H]^{+}$: Calcd. 404.1227, Found, 404.1236; Anal. Calcd. for $C_{23}H_{18}FN_3OS$ (403.47); % C, 68.47; H, 4.50; N, 10.41, Found: % C, 68.56; H, 4.69; N, 10.63.

4.1.1.11. (Z)-4-(4-methoxyphenyl)-2-(((E)-3-methylbenzylidene)hydrazinylidene)-3-phenyl-2,3-dihydrothiazole (5k):

Buff powder (yield 68%); m.p. 219-221 ^{o}C; ^{1}H NMR: δ 8.17 (s, 1H), 7.47 - 7.52 (m, 2H), 7.39 - 7.45 (m, 2H), 7.38 (d, *J* = 7.02 Hz, 1H), 7.34 (d, *J* = 7.63 Hz, 2H), 7.29 - 7.32 (m, 1H), 7.20 - 7.24 (m, 1H), 7.08 - 7.12 (m, *J* = 8.70 Hz, 2H), 6.77 - 6.82 (m, *J* = 8.70 Hz, 2H), 6.71 (s, 1H), 3.69 (s, 3H), 2.34 (s, 3H). ^{13}C NMR: δ 170.4, 159.8, 152.1, 140.5, 138.4, 137.4, 135.1, 132.1, 131.1, 130.4, 129.6, 129.3, 129.1, 127.9, 124.9, 123.0, 114.2, 102.1, 55.6, 21.5. MS (ESI) m/z: 400 $[M+H]^{+}$; HRMS (ESI) m/z $[M+H]^{+}$: Calcd. 400.1478, Found, 400.1481; Anal. Calcd. for $C_{24}H_{21}N_3OS$ (399.51); % C, 72.15; H, 5.30; N, 10.52, Found: % C, 71.94; H, 5.47; N, 10.68.

4.1.1.12. (Z)-2-(((E)-4-chlorobenzylidene)hydrazinylidene)-4-(4-methoxyphenyl)-3-phenyl-2,3-dihydrothiazole (5l):

Buff powder (yield 83%); m.p. 236-238 ^{o}C; ^{1}H NMR: δ 8.20 (s, 1H), 7.70 (d, *J* = 8.54 Hz, 2H), 7.49 (d, *J* = 8.39 Hz, 2H), 7.39 - 7.43 (m, 2H), 7.35 - 7.39 (m, 1H), 7.32 (d, *J* = 7.17 Hz, 2H), 7.08 - 7.12 (m, *J* = 8.70 Hz, 2H), 6.78 - 6.81 (m, *J* = 8.85 Hz, 2H), 6.69 (s, 1H), 3.69 (s, 3H). ^{13}C NMR: δ 170.9, 168.7, 160.0, 151.6, 150.6, 139.0, 137.9, 134.7, 134.2, 132.1, 130.4, 129.3, 129.1, 121.4, 114.2, 101.9, 55.6. MS (ESI) m/z: 420 $[M+H]^+$; HRMS (ESI) m/z $[M+H]^+$: Calcd. 420.0932, Found, 420.0938; Anal. Calcd. for $C_{23}H_{18}ClN_3OS$ (419.93); % C, 65.78; H, 4.32; N, 10.01, Found: % C, 66.04; H, 4.60; N, 10.23.

4.1.1.13. (Z)-2-(((E)-4-fluoro-3-methoxybenzylidene)hydrazinylidene)-4-(4-methoxyphenyl)-3-phenyl-2,3-dihydrothiazole (5m):

Buff powder (yield 74%); m.p. 224-226 ^{o}C; ^{1}H NMR: δ 8.21 (s, 1H), 7.47 (d, *J* = 8.09 Hz, 1H), 7.41 - 7.45 (m, 2H), 7.40 (d, *J* = 7.02 Hz, 1H), 7.36 (d, *J* = 7.17 Hz, 2H), 7.28 (d, *J* = 9.16 Hz, 2H), 7.10 (d, *J* = 8.85 Hz, 2H), 6.77 - 6.83 (m, 3H), 3.88 (s, 3H), 3.69 (s, 3H). ^{13}C NMR: δ 170.4, 168.2, 160.0, 152.0, 151.0, 147.9, 138.9, 137.2, 132.1, 130.5, 129.7, 129.2, 122.9, 121.4, 116.8, 114.2, 112.1, 102.4, 56.5, 55.6. MS (ESI) m/z: 434 $[M+H]^+$; HRMS (ESI) m/z $[M+H]^+$: Calcd. 434.1333, Found, 434.1338; Anal. Calcd. for $C_{24}H_{20}FN_3O_2S$ (433.50); % C, 66.50; H, 4.65; N, 9.69, Found: % C, 66.29; H, 4.81; N, 9.88.

4.1.1.14. 4-((E)-(((Z)-4-(4-methoxyphenyl)-3-phenylthiazol-2(3H)-ylidene)hydrazinylidene) methyl)benzonitrile (5n):

Yellowish powder (yield 85%); m.p. 238-240 ^{o}C; ^{1}H NMR NMR: δ 8.24 (s, 1H), 7.84 - 7.87 (m, 3H), 7.37 - 7.43 (m, 1H), 7.34 - 7.37 (m, 1H), 7.32 (br. s., 1H), 7.30 - 7.31 (m, 1H), 7.20 (d, *J* = 8.85 Hz, 1H), 7.10 (d, *J* = 8.85 Hz, 2H), 6.83 (d, *J* = 8.85 Hz, 1H), 6.79 (d, *J* = 8.85 Hz, 2H), 6.71 (s, 1H), 3.69 (s, 3H). ^{13}C NMR: δ 171.6, 169.5, 159.3, 149.3, 139.4, 137.0, 132.7, 131.7, 130.0, 129.1, 128.8, 128.5, 127.3, 122.5, 118.9, 113.7, 101.7, 55.1. MS (ESI) m/z: 411 $[M+H]^+$; HRMS (ESI) m/z $[M+H]^+$: Calcd. 411.1274, Found, 411.1275; Anal. Calcd. for $C_{24}H_{18}N_4OS$ (410.49); % C, 70.22; H, 4.42; N, 13.65, Found: % C, 70.43; H, 4.63; N, 13.49.

4.2. Biological evaluation

All the in vitro biological evaluation assays in the present study including NCI-USA anticancer evaluation [36], MTT cell viability assay [37,38], EGFR inhibition assay [39], cell cycle analysis [38–40], Annexin V-FITC apoptosis assay [38,41] and Western Blot Analysis [39,40] were performed as previously reported. All experimental procedures were presented in the supplementary data.

4.3. Molecular Modeling Studies

All Molecular Modeling Studies including Docking Study [32], Molecular Dynamics [39,40] and MM-PBSA Calculation and per residue contribution [35] were performed as previously reported. All detailed procedures were provided in the supplementary data.

Acknowledgement

Authors are thankful to the National Cancer Institute (NCI), developmental therapeutics program (DTP) of the United States for performing the anticancer testing. The researcher Radwan El-Haggar is funded by a postdoctoral mission from the Ministry of Higher Education of the Arab Republic of Egypt.

References

[1] R.L. Siegel, K.D. Miller, S.A. Fedewa, D.J. Ahnen, R.G.S. Meester, A. Barzi, A. Jemal, Colorectal cancer statistics, 2017, CA Cancer J Clin. 67 (2017) 177–193. https://doi.org/10.3322/caac.21395.

[2] J. Mishra, J. Dromund, S.H. Quazi, S.S. Karanki, J. Shaw, B. Chen, N. Kumar, Prospective of Colon Cancer Treatments and Scope for Combinatorial Approach to Enhanced Cancer Cell Apoptosis, Crit Rev Oncol Hematol. 86 (2013) 232–250. https://doi.org/10.1016/j.critrevonc.2012.09.014.

[3] T. Lamtha, S. Krobthong, Y. Yingchutrakul, P. Samutrtai, C. Gerner, L. Tabtimmai, K. Choowongkomon, A novel nanobody as therapeutics target for EGFR-positive colorectal cancer therapy: exploring the effects of the nanobody on SW480 cells using proteomics approach, Proteome Science. 20 (2022) 9. https://doi.org/10.1186/s12953-022-00190-6.

[4] S.V. Sharma, D.W. Bell, J. Settleman, D.A. Haber, Epidermal growth factor receptor mutations in lung cancer, Nat Rev Cancer. 7 (2007) 169–181. https://doi.org/10.1038/nrc2088.

[5] T.A. Libermann, H.R. Nusbaum, N. Razon, R. Kris, I. Lax, H. Soreq, N. Whittle, M.D. Waterfield, A. Ullrich, J. Schlessinger, Amplification, enhanced expression and possible rearrangement of EGF receptor gene in primary human brain tumours of glial origin, Nature. 313 (1985) 144–147. https://doi.org/10.1038/313144a0.

[6] T.A. Libermann, N. Razon, A.D. Bartal, Y. Yarden, J. Schlessinger, H. Soreq, Expression of epidermal growth factor receptors in human brain tumors, Cancer Res. 44 (1984) 753–760.

[7] D. Veale, T. Ashcroft, C. Marsh, G.J. Gibson, A.L. Harris, Epidermal growth factor receptors in non-small cell lung cancer., Br J Cancer. 55 (1987) 513–516.

[8] D.A. Sabbah, R. Hajjo, K. Sweidan, Review on Epidermal Growth Factor Receptor (EGFR) Structure, Signaling Pathways, Interactions, and Recent Updates of EGFR Inhibitors, Curr Top Med Chem. 20 (2020) 815–834. https://doi.org/10.2174/1568026620666200303123102.

[9] R. Roskoski, Small molecule inhibitors targeting the EGFR/ErbB family of protein-tyrosine kinases in human cancers, Pharmacological Research. 139 (2019) 395–411. https://doi.org/10.1016/j.phrs.2018.11.014.

[10] L. Huang, S. Jiang, Y. Shi, Tyrosine kinase inhibitors for solid tumors in the past 20 years (2001–2020), Journal of Hematology & Oncology. 13 (2020) 143. https://doi.org/10.1186/s13045-020-00977-0.

[11] D. Westover, J. Zugazagoitia, B.C. Cho, C.M. Lovly, L. Paz-Ares, Mechanisms of acquired resistance to first- and second-generation EGFR tyrosine kinase inhibitors, Ann Oncol. 29 (2018) i10–i19. https://doi.org/10.1093/annonc/mdx703.

[12] M.M. Attwood, D. Fabbro, A.V. Sokolov, S. Knapp, H.B. Schiöth, Trends in kinase drug discovery: targets, indications and inhibitor design, Nat Rev Drug Discov. 20 (2021) 839–861. https://doi.org/10.1038/s41573-021-00252-y.

[13] T.R. Rheault, J.C. Stellwagen, G.M. Adjabeng, K.R. Hornberger, K.G. Petrov, A.G. Waterson, S.H. Dickerson, R.A. Mook, S.G. Laquerre, A.J. King, O.W. Rossanese, M.R. Arnone, K.N. Smitheman, L.S. Kane-Carson, C. Han, G.S. Moorthy, K.G. Moss, D.E. Uehling, Discovery of Dabrafenib: A Selective Inhibitor of Raf Kinases with Antitumor Activity against B-Raf-Driven Tumors, ACS Med. Chem. Lett. 4 (2013) 358–362. https://doi.org/10.1021/ml4000063.

[14] J. Das, P. Chen, D. Norris, R. Padmanabha, J. Lin, R.V. Moquin, Z. Shen, L.S. Cook, A.M. Doweyko, S. Pitt, S. Pang, D.R. Shen, Q. Fang, H.F. de Fex, K.W. McIntyre, D.J. Shuster, K.M. Gillooly, K. Behnia, G.L. Schieven, J. Wityak, J.C. Barrish, 2-Aminothiazole as a Novel Kinase Inhibitor Template. Structure−Activity Relationship Studies toward the Discovery of N-(2-Chloro-6-methylphenyl)-2-[[6-[4-(2-hydroxyethyl)-1- piperazinyl)]-2-methyl-4-pyrimidinyl]amino)]-1,3-thiazole-5-carboxamide (Dasatinib, BMS-354825) as a Potent pan-Src Kinase Inhibitor, J. Med. Chem. 49 (2006) 6819–6832. https://doi.org/10.1021/jm060727j.

[15] A. Ayati, S. Emami, S. Moghimi, A. Foroumadi, Thiazole in the targeted anticancer drug discovery, Future Medicinal Chemistry. 11 (2019) 1929–1952. https://doi.org/10.4155/fmc-2018-0416.

[16] S. Li, G. Luan, X. Ren, W. Song, L. Xu, M. Xu, J. Zhu, D. Dong, Y. Diao, X. Liu, L. Zhu, R. Wang, Z. Zhao, Y. Xu, H. Li, Rational Design of Benzylidenehydrazinyl-Substituted Thiazole Derivatives as Potent Inhibitors of Human Dihydroorotate Dehydrogenase with in Vivo Anti-arthritic Activity, Sci Rep. 5 (2015) 14836. https://doi.org/10.1038/srep14836.

[17] Y. Zhang, X. Fu, Y. Yan, J. Liu, Microwave-assisted synthesis and biological evaluation of new thiazolylhydrazone derivatives as tyrosinase inhibitors and antioxidants, Journal of Heterocyclic Chemistry. 57 (2020) 991–1002. https://doi.org/10.1002/jhet.3760.

[18] L.T. Maillard, S. Bertout, O. Quinonéro, G. Akalin, G. Turan-Zitouni, P. Fulcrand, F. Demirci, J. Martinez, N. Masurier, Synthesis and anti-Candida activity of novel 2-hydrazino-1,3-thiazole derivatives, Bioorganic and Medicinal Chemistry Letters. 23 (2013) 1803–1807. https://doi.org/10.1016/j.bmcl.2013.01.039.

[19] A. Kryshchyshyn, D. Kaminskyy, O. Karpenko, A. Gzella, P. Grellier, R. Lesyk, Thiazolidinone/thiazole based hybrids – New class of antitrypanosomal agents, European Journal of Medicinal Chemistry. 174 (2019) 292–308. https://doi.org/10.1016/j.ejmech.2019.04.052.

[20] M. D'Ascenzio, B. Bizzarri, C. De Monte, S. Carradori, A. Bolasco, D. Secci, D. Rivanera, N. Faulhaber, C. Bordón, L. Jones-Brando, Design, synthesis and biological characterization of thiazolidin-4-one derivatives as promising inhibitors of Toxoplasma gondii, European Journal of Medicinal Chemistry. 86 (2014) 17–30. https://doi.org/10.1016/j.ejmech.2014.08.046.

[21] O.P. Kovalenko, G.P. Volynets, M.Y. Rybak, S.A. Starosyla, O.I. Gudzera, S.S. Lukashov, V.G. Bdzhola, S.M. Yarmoluk, H.I. Boshoff, M.A. Tukalo, Dual-target inhibitors of mycobacterial aminoacyl-tRNA synthetases among N-benzylidene-N′-thiazol-2-yl-hydrazines, Med. Chem. Commun. 10 (2019) 2161–2169. https://doi.org/10.1039/C9MD00347A.

[22] P. Makam, R. Kankanala, A. Prakash, T. Kannan, 2-(2-Hydrazinyl)thiazole derivatives: Design, synthesis and in vitro antimycobacterial studies, European Journal of Medicinal Chemistry. 69 (2013) 564–576. https://doi.org/10.1016/j.ejmech.2013.08.054.

[23] H.R.M. Rashdan, M. El-Naggar, A.H. Abdelmonsef, Synthesis, Molecular Docking Studies and In Silico ADMET Screening of New Heterocycles Linked Thiazole Conjugates as Potent Anti-Hepatic Cancer Agents, Molecules. 26 (2021) 1705. https://doi.org/10.3390/molecules26061705.

[24] A.S. Filimonov, A.A. Chepanova, O.A. Luzina, A.L. Zakharenko, O.D. Zakharova, E.S. Ilina, N.S. Dyrkheeva, M.S. Kuprushkin, A.V. Kolotaev, D.S. Khachatryan, J. Patel, I.K.H. Leung, R. Chand, D.M. Ayine-Tora, J. Reynisson, K.P. Volcho, N.F. Salakhutdinov, O.I. Lavrik, New Hydrazinothiazole Derivatives of Usnic Acid as Potent Tdp1 Inhibitors, Molecules. 24 (2019) E3711. https://doi.org/10.3390/molecules24203711.

[25] Z. Zhao, H. Wu, L. Wang, Y. Liu, S. Knapp, Q. Liu, N.S. Gray, Exploration of Type II Binding Mode: A Privileged Approach for Kinase Inhibitor Focused Drug Discovery?, ACS Chem. Biol. 9 (2014) 1230–1241. https://doi.org/10.1021/cb500129t.

[26] Y. Liu, N.S. Gray, Rational design of inhibitors that bind to inactive kinase conformations, Nat Chem Biol. 2 (2006) 358–364. https://doi.org/10.1038/nchembio799.

[27] V. Gandin, A. Ferrarese, M. Dalla Via, C. Marzano, A. Chilin, G. Marzaro, Targeting kinases with anilinopyrimidines: discovery of N-phenyl-N'-[4-(pyrimidin-4-ylamino)phenyl]urea derivatives as selective inhibitors of class III receptor tyrosine kinase subfamily, Sci Rep. 5 (2015) 16750. https://doi.org/10.1038/srep16750.

[28] R. Cirilli, R. Ferretti, F. La Torre, D. Secci, A. Bolasco, S. Carradori, M. Pierini, High-performance liquid chromatographic separation of enantiomers and diastereomers of 2-methylcyclohexanone thiosemicarbazone, and determination of absolute configuration and configurational stability, Journal of Chromatography A. 1172 (2007) 160–169. https://doi.org/10.1016/j.chroma.2007.10.009.

[29] W.-D. Pfeiffer, K.-D. Ahlers, A.S. Saghyan, A. Villinger, P. Langer, Unexpected Ring Enlargement of 2-Hydrazono-2,3-dihydro-1,3-thiazoles to 1,3,4-Thiadiazines, Helvetica Chimica Acta. 97 (2014) 76–87. https://doi.org/10.1002/hlca.201300077.

[30] H.M. Aly, N.M. Saleh, H.A. Elhady, Design and synthesis of some new thiophene, thienopyrimidine and thienothiadiazine derivatives of antipyrine as

potential antimicrobial agents, European Journal of Medicinal Chemistry. 46 (2011) 4566–4572. https://doi.org/10.1016/j.ejmech.2011.07.035.

[31] JohnC. Reed, JulianeM. Jurgensmeier, S. Matsuyama, Bcl-2 family proteins and mitochondria, Biochimica et Biophysica Acta (BBA) - Bioenergetics. 1366 (1998) 127–137. https://doi.org/10.1016/S0005-2728(98)00108-X.

[32] S. Vilar, G. Cozza, S. Moro, Medicinal Chemistry and the Molecular Operating Environment (MOE): Application of QSAR and Molecular Docking to Drug Discovery, Current Topics in Medicinal Chemistry. 8 (n.d.) 1555–1572.

[33] J. Stamos, M.X. Sliwkowski, C. Eigenbrot, Structure of the Epidermal Growth Factor Receptor Kinase Domain Alone and in Complex with a 4-Anilinoquinazoline Inhibitor *, Journal of Biological Chemistry. 277 (2002) 46265–46272. https://doi.org/10.1074/jbc.M207135200.

[34] M.J. Abraham, T. Murtola, R. Schulz, S. Páll, J.C. Smith, B. Hess, E. Lindahl, GROMACS: High performance molecular simulations through multi-level parallelism from laptops to supercomputers, SoftwareX. 1–2 (2015) 19–25. https://doi.org/10.1016/j.softx.2015.06.001.

[35] R. Kumari, R. Kumar, Open Source Drug Discovery Consortium, A. Lynn, g_mmpbsa--a GROMACS tool for high-throughput MM-PBSA calculations, J Chem Inf Model. 54 (2014) 1951–1962. https://doi.org/10.1021/ci500020m.

[36] NCI-60 Screening Methodology | NCI-60 Human Tumor Cell Lines Screen | Discovery & Development Services | Developmental Therapeutics Program (DTP), (n.d.). https://dtp.cancer.gov/discovery_development/nci-60/methodology.htm (accessed July 14, 2022).

[37] W.M. Eldehna, A.M. El Kerdawy, G.H. Al-Ansary, S.T. Al-Rashood, M.M. Ali, A.E. Mahmoud, Type IIA - Type IIB protein tyrosine kinase inhibitors hybridization as an efficient approach for potent multikinase inhibitor development: Design, synthesis, anti-proliferative activity, multikinase inhibitory activity and molecular modeling of novel indolinone-based ureides and amides, Eur J Med Chem. 163 (2019) 37–53. https://doi.org/10.1016/j.ejmech.2018.11.061.

[38] I.H. Eissa, R. El-Haggar, M.A. Dahab, M.F. Ahmed, H.A. Mahdy, R.I. Alsantali, A. Elwan, N. Masurier, S.S. Fatahala, Design, synthesis, molecular modeling and biological evaluation of novel Benzoxazole-Benzamide conjugates via a 2-Thioacetamido linker as potential anti-proliferative agents, VEGFR-2 inhibitors and apoptotic inducers, Journal of Enzyme Inhibition and Medicinal Chemistry. 37 (2022) 1587–1599. https://doi.org/10.1080/14756366.2022.2081844.

[39] M.F. Ahmed, E.Y. Santali, Discovery of pyridine- sulfonamide hybrids as a new scaffold for the development of potential VEGFR-2 inhibitors and apoptosis

inducers, Bioorganic Chemistry. 111 (2021) 104842. https://doi.org/10.1016/j.bioorg.2021.104842.

[40] M.F. Ahmed, E.Y. Santali, R. El-Haggar, Novel piperazine–chalcone hybrids and related pyrazoline analogues targeting VEGFR-2 kinase; design, synthesis, molecular docking studies, and anticancer evaluation, Journal of Enzyme Inhibition and Medicinal Chemistry. 36 (2021) 308–319. https://doi.org/10.1080/14756366.2020.1861606.

[41] K.K.-W. Lo, T.K.-M. Lee, J.S.-Y. Lau, W.-L. Poon, S.-H. Cheng, Luminescent biological probes derived from ruthenium(II) estradiol polypyridine complexes, Inorg Chem. 47 (2008) 200–208. https://doi.org/10.1021/ic701735q.